SANDIA REPORT

SAND2017-12869
Unlimited Release
Printed September 2015

Verification Tests for Sierra/SM's Reproducing Kernal Particle Method

Brian D. Giffin

Prepared by
Sandia National Laboratories
Albuquerque, New Mexico 87185 and Livermore, California 94550

Sandia National Laboratories is a multi-program laboratory managed and operated by Sandia Corporation, a wholly owned subsidiary of Lockheed Martin Corporation, for the U.S. Department of Energy's National Nuclear Security Administration under contract DE-AC04-94AL85000.

Sandia National Laboratories

Issued by Sandia National Laboratories, operated for the United States Department of Energy by Sandia Corporation.

Available to DOE and DOE contractors from
U.S. Department of Energy
Office of Scientific and Technical Information
P.O. Box 62
Oak Ridge, TN 37831

Telephone: (865) 576-8401
Facsimile: (865) 576-5728
E-Mail: reports@adonis.osti.gov
Online ordering: http://www.osti.gov/bridge

Available to the public from
U.S. Department of Commerce
National Technical Information Service
5285 Port Royal Rd
Springfield, VA 22161

Telephone: (800) 553-6847
Facsimile: (703) 605-6900
E-Mail: orders@ntis.fedworld.gov
Online ordering: http://www.ntis.gov/help/ordermethods.asp?loc=7-4-0#online

SAND2017-12869
Unlimited Release
Printed September 2015

Verification Tests for Sierra/SM's Reproducing Kernal Particle Method

Brian D. Giffin
Computational Structural Mechanics and Applications
Sandia National Laboratories
P.O. Box 5800
Albuquerque, NM 87185-0840
bdgiffi@sandia.gov

Abstract

This report seeks to verify the proper implemention of RKPM within Sierra by comparing the results from several basic example problems excecuted with RKPM against the analytical and FEM solutions for these same problems. This report was compiled as a summer student intern project.

Acknowledgments

Many thanks to Dr. Josesph E. Bishop, Dr. David J. Littlewood for their guidance and support in assembling this report.

Also thanks to Dr. Elilot Fang and Dr. Joseph Jung for their support of the project.

The team of inidivuals at UCLA responsible for the impelementation of the RKPM code are deserving of recognition for their work, without which this report would not have been possible. A special thanks to Mike Hillman and Edouard Yreux, and very special thanks to Dr. J. S. Chen.

Contents

Preface **9**

Summary **10**

Introduction 11

One-Dimensional Steel Bar Under Axial Gravity Loading 11

Purpose 11

Description of Model 11

Analytical Predictions 12

Test Procedure 12

Results 13

Conclusions 19

Cantilever Beam Subjected to an End-Shear Load 20

Purpose 20

Description of Model 20

Analytical Predictions 20

Test Procedure 22

Results 22

Conclusions 27

Prismatic Shaft in Pure Torsion 28

Purpose 28

Description of Model 28

Analytical Predictions 28

Test Procedure 29
Results 30
Conclusions 34

References **35**

List of Figures

1 One-Dimensional Bar Idealization 12

2 Comparison of Bar Stresses 13

3 Comparison of Bar Displacements 13

4 Viscously Damped Tip Displacement ($u_{zz}(L)$) vs. Time 14

5 Bar Displacement and Stress vs. Z 14

6 Normalized Absolute Error of Bar Displacement ($u_{zz}(Z)$) vs. Z 15

7 Bar Displacement ($u_{zz}(Z)$) vs. Z with Variable Support Size 16

8 Bar Stress ($\sigma_{zz}(Z)$) vs. Z with Refinement 17

9 Bar L^2 and Energy Norms 18

10 Comparison of Undamped Tip Displacement ($u_{zz}(L)$) vs. Time. 19

11 Prismatic Beam Idealization 21

12 Comparison of Beam Stresses 23

13 Comparison of Beam Displacements 23

14 Beam Displacement and Stress Plots 24

15 Beam Normalized Aboslute Displacement Error 25

16 Beam Normalized L^2 Displacement Norm 25

17 Beam Energy Errors 26

18 Beam Normalized Energy Norm 27

19 Prismatic Shaft Idealization 29

20 Comparison of Shaft Stresses 30

21 Comparison of Shaft Displacements 30

22 Beam Displacement and Stress Plots 31

23 Beam Normalized Aboslute Displacement Error 31
24 Shaft Normalized L^2 Displacement Norm 32
25 Beam Energy Errors 33
26 Beam Normalized Energy Semi-Norm 33

Preface

Finite element methods currently in use provide a powerful means of performing complex simulations for practical applications. However, while the analysis procedures for these methods are robust and well established, they nonetheless rely on the user to properly assemble a meshed model. Not only is this a time consuming process, but it is also prone to errors in the meshing procedure. What's more, standard meshed analyses may encounter difficulties with simulations involving large deformations, fracture, or impact.

It therefore becomes of interest to investigate the possiblities of implementing so-called "meshless" methods of analysis. Namely, the reproducing kernal particle method (RKPM) provides a promising solution to many of the aforementioned issues with finite elements. Implementation of RKPM analysis procedures within the explicit dynamics module (formerly Presto) in Sierra/SM is currently underway.

It should be noted that Sierra's RKPM analysis methods are still a work in progress, and that the results of the following examples may bring to light certain issues with the implementation that may need to be resolved. This report is intended to demonstrate not just the current capabilities of RKPM within Sierra, but its current limitations, as well. Identifying problems with the code is the first step to fixing them, and it is hoped that this report can assist with this process.

Summary

The report first explores three main examples, provided with a description of the model parameters. Analysis Results are compared against the analytical and FEM solutions for each problem. Some simple variable sensitivity and mesh refinement studies are provided as well. Finally, hypotheses regarding potential sources of error are put forth for consideration.

Introduction

The following verification tests are intended to demonstrate the current capabilities of Sierra/SM's Reproducing Kernal Particle Method of analysis. The scope of these tests focused on confirmed aspects of the code to have been implemented. The report is divided into three sections, each based upon the test that was performed.

One-Dimensional Steel Bar Under Axial Gravity Loading

Purpose

The purpose of this test was to verify that the RKPM implementation within Sierra/SM can accurately solve for the displacement and stress fields of a unidimensional body subjected to a gravity field boundary condition. The chosen model parameters and support conditions are kept as simple as possible for the sake of easily deriving exact solutions for comparison. Results are also compared against an analogous hex mesh model in Sierra.

Description of Model

The model consisted of an axial bar with square cross-section, restrained by a fixed set of nodes at one end. The material was modeled as having linear-elastic behavior using the 'neo_hookean' material model, and having the material properties of a typical mild steel. The Poisson's ratio for the material was set to zero to make the problem fully one-dimensional. All units for the model definitions and analysis results are listed in standard SI units: kilograms, meters, seconds.

The bar was subjected to a gravity field boundary condition with a gravitational constant of $9.8\frac{m}{s^2}$. The field was directed such that it induced only axial tension within the bar. In a quasi-static state, the force of gravity acting over the bar was expected to result in a linear stress field and a quadratic displacement field. Both fields would vary only with axial position along the length of the bar.

Since the capabilities for RKPM are not yet available within the Adagio Sierra module, the analysis had to be run as a Presto procedure. The gravity field was instructed to become active during the initial timestep within the analysis. Viscous damping was introduced within the model to help the bar reach an approximately quasi-static condition. Sufficient time was allowed for the bar to achieve this state.

Analytical Predictions

The one-dimensional bar can be represented by the idealization in Figure 1.

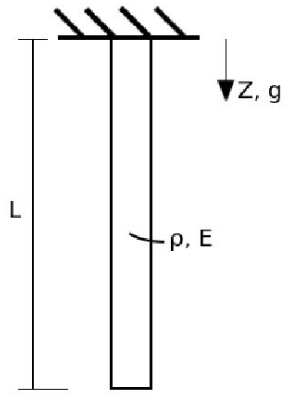

Figure 1. One-Dimensional Bar Idealization

Volume effects have been neglected to match the numerical model definition. As a result, formulation of the analytical stress and displacement fields is trivial. The resulting exact equations for axial stress (Equation 1) and displacement (Equation 2) in the Lagrangian reference frame are provided below.

$$\sigma_{zz}(Z) = \rho g(L - Z) \tag{1}$$

$$u_{zz}(Z) = \frac{\rho g}{E}(L \cdot Z - \frac{Z^2}{2}) \tag{2}$$

Test Procedure

An initial hex mesh of the bar was modeled within Cubit, and later converted to an RKPM model through the 'spheregen.py' script. The bar was meshed such that the resulting square cross-section consisted of four elements, having two elements on each side.

The 'support size' parameter included within the Sierra RKPM block required a value larger than 1.5. The parameter itself is a scale factor for the size of the RK support function. The minimum value of 1.5 is required to ensure that enough neighboring nodes are included within the support function for each inidividual node. A sensitivity analysis of this parameter was carried out to investiage the effects of varying 'support size' within the Sierra input file.

In general, even with a larger specified user time step for the RKPM model, the runtime for the meshed analysis was consistently faster. Energy and errors would return as 'nan' if the time step was set too high. At least in this instance, the allowable time steps for the hex mesh model and the RKPM model were comparable.

Results

A visualization of the results for the axial bar are shown in figures 2(a) and 2(b).

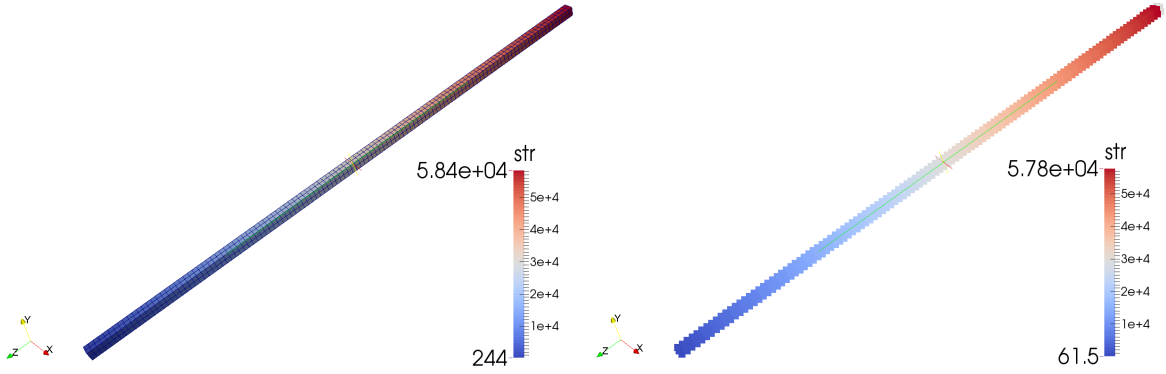

(a) **(b)**

Figure 2. Comparison of axial stresses in the shaft for (a) FEM and (b) RKPM

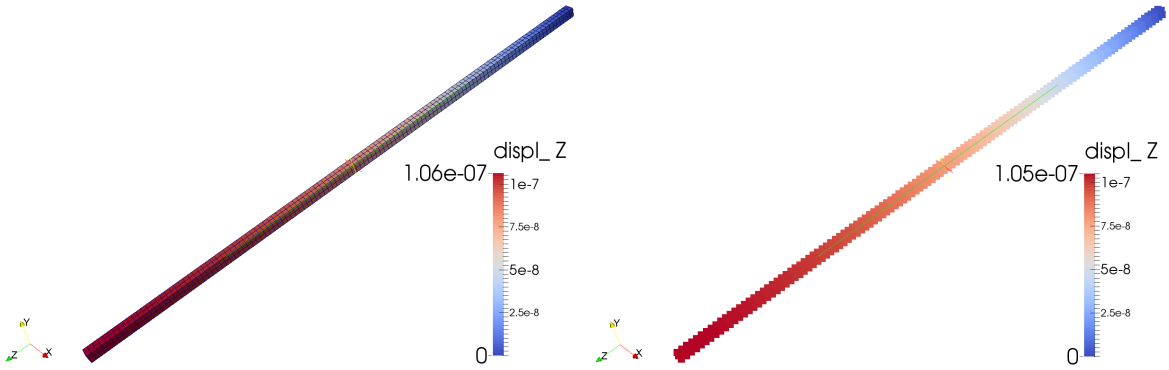

(a) **(b)**

Figure 3. Comparison of axial displacement in the bar for (a) FEM and (b) RKPM

The RKPM parameters of interest for tip displacement vs time, bar displacement vs Z, and bar stress vs Z were compared with the analytical and hex mesh model results. Plots depicting these comparions may be found in Figures 4, 5(a), and 5(b), respectively.

As anticipated, the analytical and hex mesh model results correspond almost exactly. However, the RKPM results differ from the analytical results by as much as 1.25% for displacement at the tip, and by 50.0% for stress at the base.

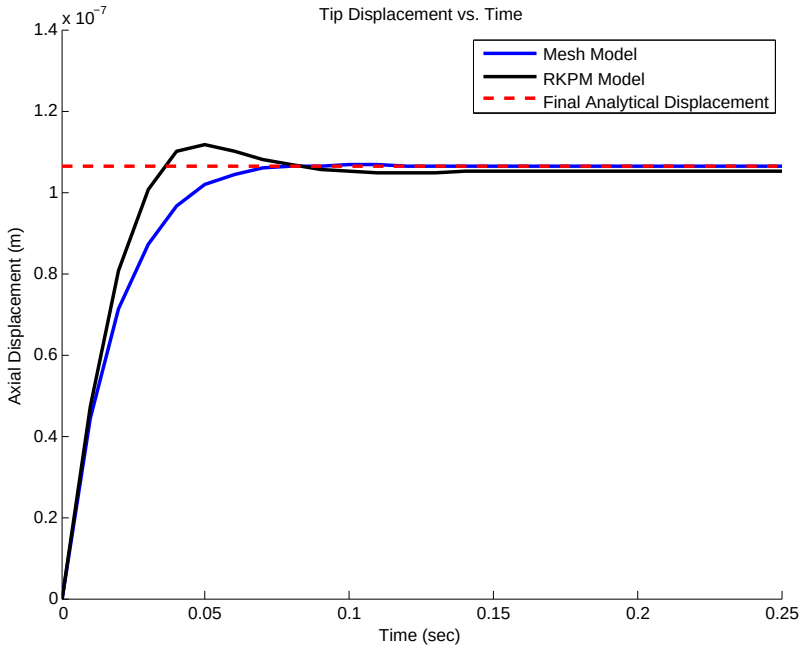

Figure 4. Comparison of Viscously Damped Tip Displacement ($u_{zz}(L)$) vs. Time

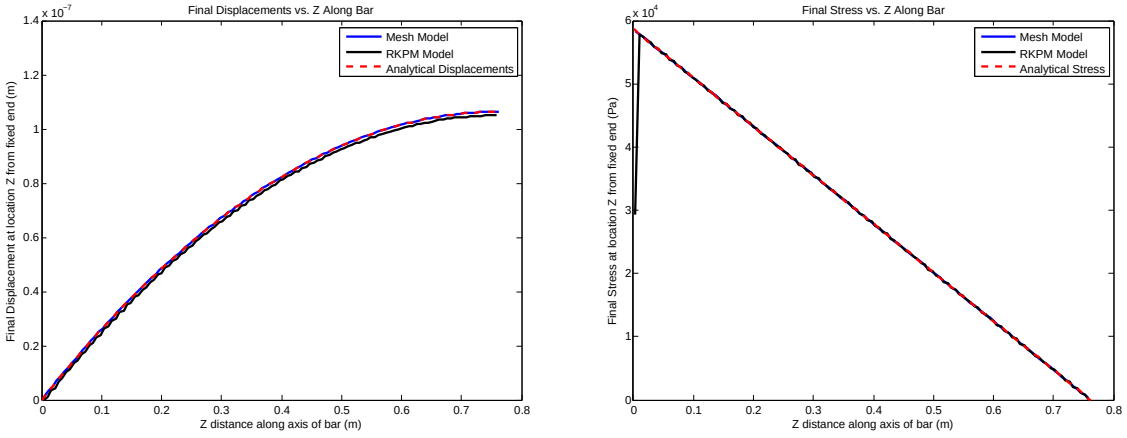

(a) **(b)**

Figure 5. (a) Comparison of bar displacement ($u_{zz}(Z)$) vs. Z (b) and axial bar stress ($\sigma_{zz}(Z)$) vs. Z

For these comparisons, it should be noted that a direct node-to-node comparison could not be made, due to the method used to convert meshed models into sphere based RKPM models. For converting a hex mesh into a set of sphere elements, the current process generates RKPM elements/nodes at the centroid of each hex element. Thus, values at inidivual nodes between the hex mesh and RKPM models could not be made. This is significant in that tip displcament could not be measured at a node located the full distance 'L' from the support in the RKPM model, but rather at the nearest element/node, which falls short of this distance by one half the size of an individual element. Therefore, a more accurate representation of the results may be observed in the plots for displacement and stress vs Z (see Figures 5(a) and 5(b).) Despite this discrepancy, the results for the tip displacement are still comparable for finer meshes.

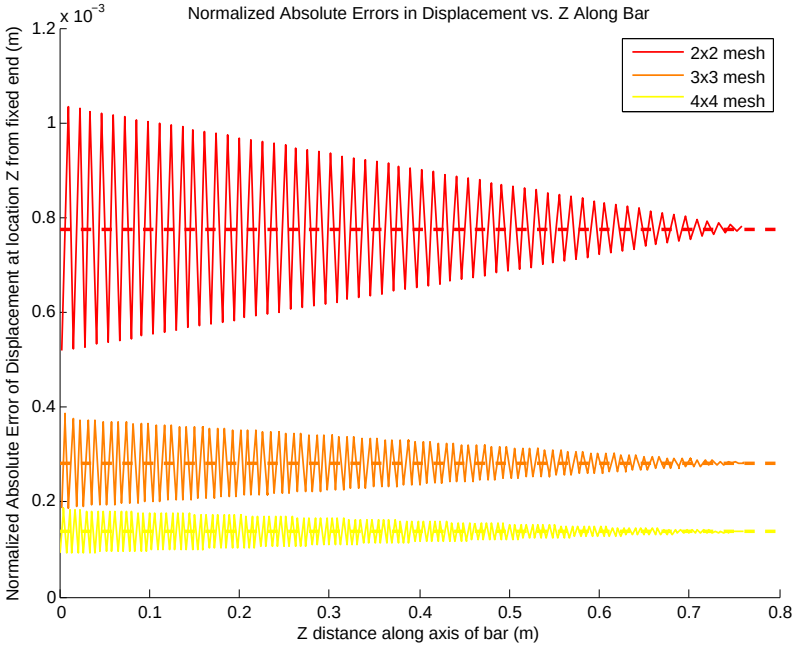

Figure 6. Comparison of normalized absolute errors in bar displacement ($||u^h_{zz}(Z) - u_{zz}(Z)||$) vs. Z with increasing mesh refinement. Dashed lines represent the averaged error in the displacement over the length of the bar.

The method for assigning the fixed displacement condition at the supported end of the bar should also be considered in our review of the results. Within the RKPM model, the imposed fixed displacements are applied to the corresponding particle elements at the supported end. These particles, having been generated at the centroid of each hex element in the conversion process, are therefore offset from the intended location of fixity by one half of the distance between particles. The inherrent error in the results that this method of assignment produces is apparent upon observing the convergence pattern for the displacement absolute errors, shown in Figure 6.

Based on these differences in the model results, development of a method for converting meshed model nodes into sphere elements might help to remedy these issues.

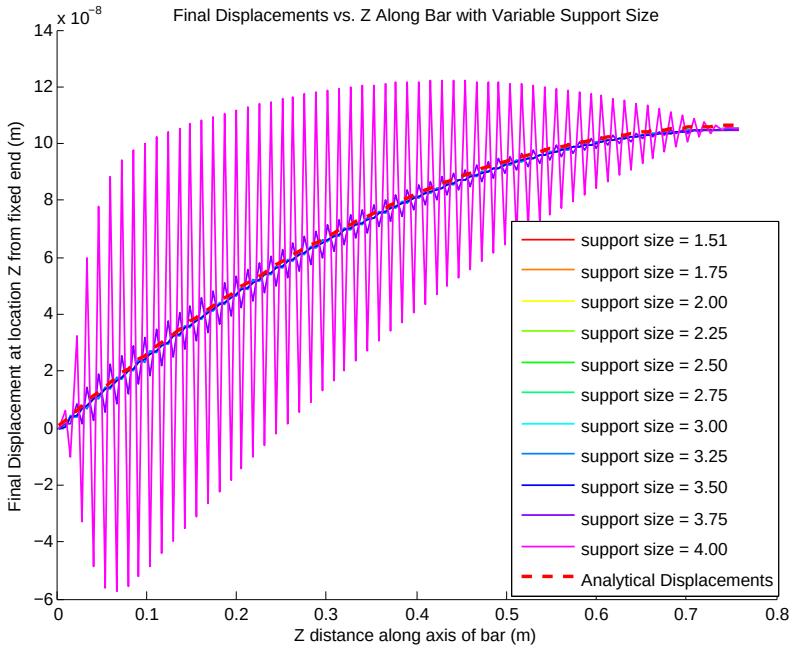

Figure 7. Comparison of Bar Displacement ($u_{zz}(Z)$) vs. Z with increasing support size

From Figure 6, we see that the error in the displacement values in the RKPM model oscillates about an average error value. If we normalize the magnitude of the averaged error by the size of each element, we find that there is a distinct correlation between element size and displacement error. In other words, the magnitude of the average displacement error is directly proportional to element size. We would therefore expect to see more accurate results with increasing mesh refinement, yielding a linear convergence rate.

Also interesting to note is the apparent instability of the displacement values in the RKPM model. Particularly, the displacement error appears to regularly fluctuate about the average error, and increasingly so at locations in the bar closer to the fixed support. Residual inertial effects within the bar may contribute to this phenomenon, though it is more likely that it is caused by an inherrent numerical instability. The manually defined time step for the problem was selected to avoid prohibitively long analysis times. However, it is entirely possible that the problem may be associated with a supercritical, or near supercritical time step. SPH particle method analyses in Sierra have been known to experience instabilities at the default time step, occasionally causing the SPH material to invert. While RKPM is expected to provide more stable results when compared to SPH, it may still be vulnerable to the same issues.

A sensitivity analysis of the 'support size' input parameter for Sierra was conducted to further investigate the source of the instability. The results indicated that increasing the support size while leaving the user defined time step the same tended to amplify the observed instability, ultimately leading to material inversion. Figure 7 depicts the variability in bar displacements with respect to

increasing support size.

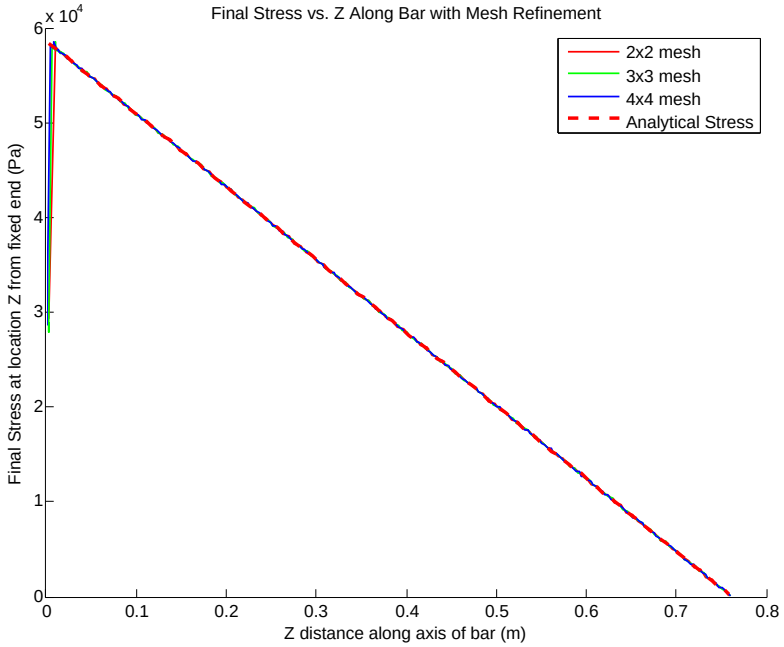

Figure 8. Comparison of Bar Stress ($\sigma_{zz}(Z)$) vs. Z with increasing mesh refinement.

Ordinarily, increasing the support size should improve the accuracy of the results, but it requires that the time step also be reduced. We may may therefore expect to see increasing instability in our results. Of peculiar interest, however, is that specifying a reduced time step in the original model appeared to have no effect whatsoever on the observed instability. This may provide evidence against the hypothesis that a large time step is the major source of the problem.

For the most part, results for axial stress within the bar were considerably more accurate. Stress percent errors between the exact and RKPM model results observed at most locations along the length of the bar were within the range of 0.25%. Yet again, major discrepancies in the results can be attributed to the nature of the model's definition. Since the node/element at the free end of the bar experiences near zero stress, and because it falls short of the full length of the bar by half the length of one element, the stress percent error at the free end appears to blow up, but the absolute error remains essentially the same. The stress near the base of the bar for the RKPM model was dramatically less than that of the analytical and meshed models. This may or may not be related to the method used to assign fixed nodes for the RKPM model. Since the nodes at the base of the bar double as elements, and considering that these nodes have been assigned prescribed displacements, it is possible that the error in the results may stem from the assignment of essential boundary conditions. As can be observed in Figure 8, no improvement in this error at the end node is obtained from mesh refinement.

Looking at the convergence rates with increasing mesh refinement for the normalized L^2 dis-

placement and normalized energy semi-norms in figure 9, we see that the convergence rates for RKPM are approximately half of what we would expect for FEM (two-to-one for the L^2 norm, one-to-one for the energy norm). It may be that the decreased convergence rates may be related to the stresses at the boundary conditions, though it is surprising the results are almost exactly one half of the FEM convergence rates.

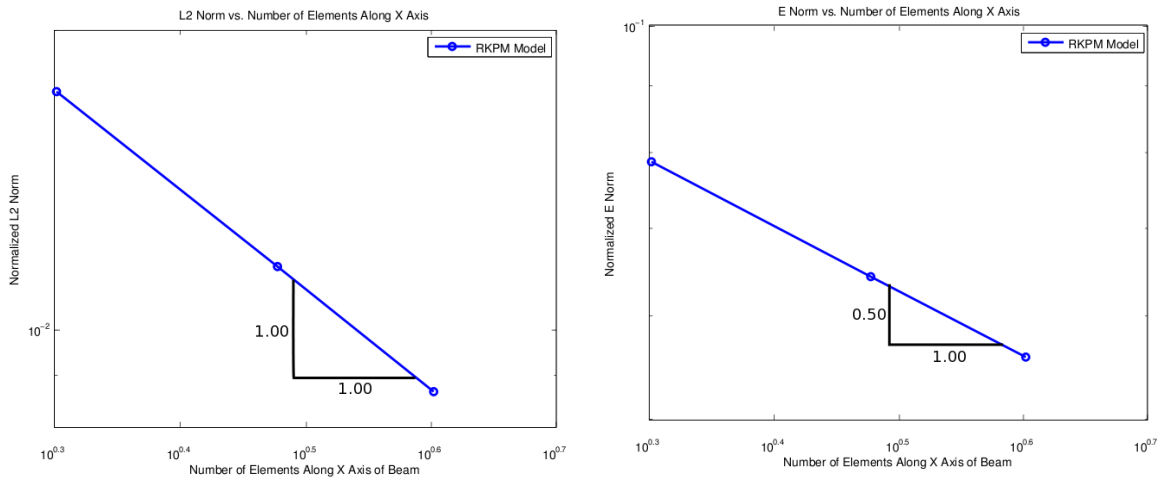

(a) **(b)**

Figure 9. (a) Normalized L^2 displacement norm and (b) normalized energy norm vs. number of elements along the z direction of the bar.

Of further interest is the observed difference in the dynamic response of the two simulated models. While a more in-depth analysis of the dynamics of the bar models is beyond the scope of this investigation, it is nonetheless interesting to note that the dominant elastic period of the bar in the meshed model is larger than that of the bar in the RKPM model. Figure 10 illustrates this comparison, showing the undamped response of the two models. Based on these shapes, a rough estimate of the dominant frequency can be made, with the finding that the meshed model's response had an approximate frequency of $3.125Hz$, whereas the RKPM model's response was at $7.143Hz$.

However, this may only be the result of having a low resolution mesh. The results from the limited refinement study implied that the frequency of the RKPM model's response may apporach the results of the meshed model with further mesh refinement. A more detailed experiment comparing observed periods of oscillation between meshed and RKPM models would be warranted to support this hypothesis.

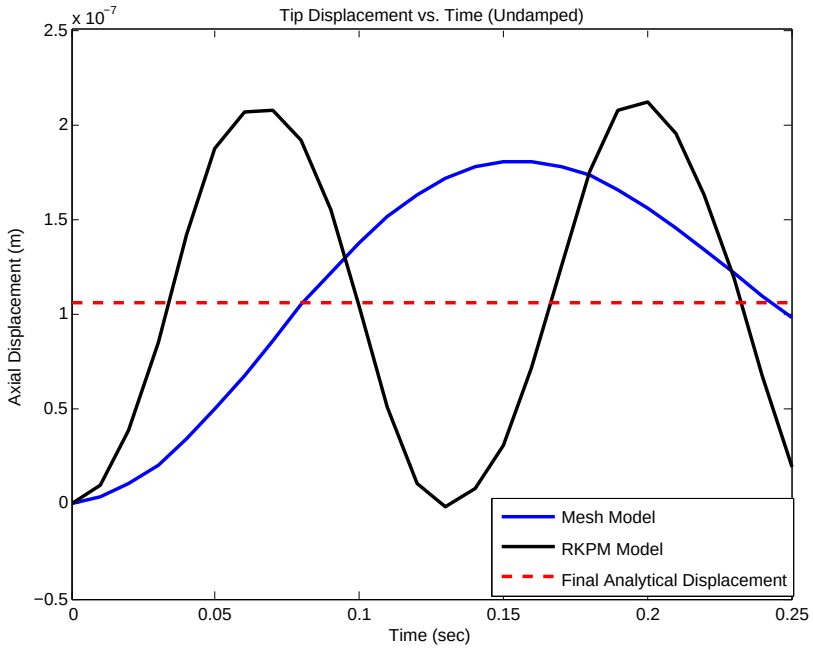

Figure 10. Comparison of Undamped Tip Displacement ($u_{zz}(L)$) vs. Time.

Conclusions

While the results of the test at the very least appear to produce reasonable values for both displacement and stress fields within the bar, there appear to be some inherrent inconsistencies in the results that are likely related to the current method of defining and assigning essential boundary conditions for sphere based elements. Displacements appear to be offset from the expected solution by an amount proportional to the mesh size, and stress appears to experience a dramatic drop at the location where displacement boundary conditions have been imposed. Some amount of instability was also observed in the model that may be linked to the choice of time step, and possibly support size. An investigation of dynamics within RKPM may be in order given the difference in elastic response between the hex and sphere based models, though this may simply require greater mesh refinement to remedy.

Cantilever Beam Subjected to an End-Shear Load

Purpose

This test was intended to verify RKPM's ability to model linear elastic behavior of three dimensional solid bodies. The example problem in question focused on the bending behavior of a prismatic cantilever beam subjected to an end-shear load. The resulting displacement and stress fields were compared against the exact solutions from elasticity theory for infinitesimally small strains. Results are also compared against an analogous hex mesh model of the same problem.

Description of Model

The model consisted of a prismatic beam, contrained at both ends by two nodesets with prescribed displacements consistent with the exact displacement field. The material was modeled as having linear-elastic behavior using the 'neo_hookean' material model, and having the material properties of a typical mild steel. The Poisson's ratio for the material was set to 0.3 to allow for volumetric effects. All units for the model definitions and analysis results were listed in standard SI units: kilograms, meters, seconds.

The applied displacement boundary conditions were intended to induce a stress field corresponding to the application of an end-shear load at one end of the beam, with the opposite end fixed (weakly). Applied displacements were made sufficiently small so that the model's behavior could be closely approximated by the condition of infinitesimally small strains. The exact solutions for the resulting stress and displacement fields are provided in the following section.

As with the axial bar problem, the analysis was executed through Sierra/SM's explicit dynamics module (formerly Presto). The displacements at the ends of the beam were increased from zero to the absolute displacement values with a time varying linear ramp function. Viscous damping was introduced within the model to help the beam reach an approximately quasi-static condition. Sufficient time was allowed for the beam to achieve this state.

Analytical Predictions

The prismatic beam with its corresponding coordinate system and imposed loading can be represented by the idealization in Figure 11.

Full 3-D elasticity solutions for the resulting stress and displacement fields were derived for the case of infinitesimally small strains. The equations given below were provided by Dr. Joseph E. Bishop, specifically from his article entitled "A Displacement-Based Finite Element Formulation for General Polyhedra using Harmonic Shape Functions."

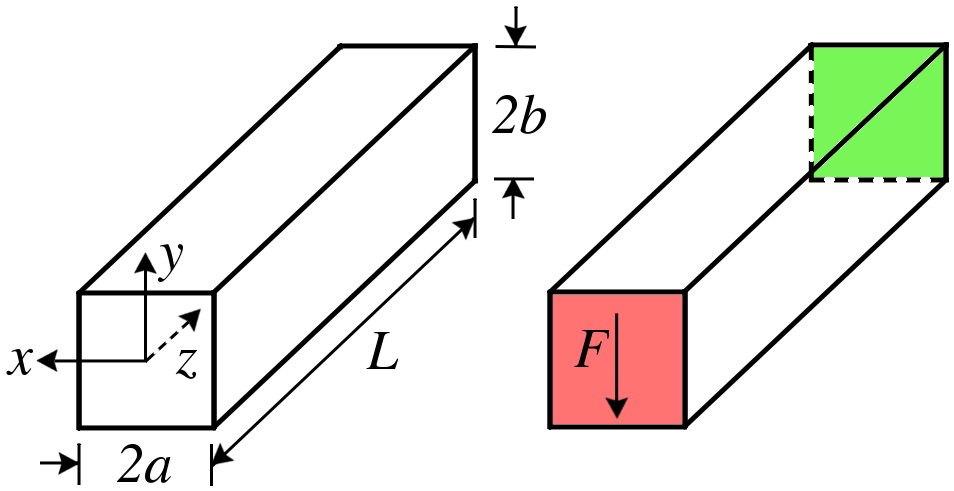

Figure 11. Prismatic Beam Idealization: Coordinate system and relevant dimensions are depicted at left. The surface at $z = L$ (highlighted green) is fixed (weakly). The surface at $z = 0$ (highlighted red) is subjected to a uniformly distributed shear load F in the negative y direction.

$$\sigma_{xx} = \sigma_{yx} = \sigma_{yy} = 0 \tag{3}$$

$$\sigma_{zz} = \frac{F}{I} yz \tag{4}$$

$$\sigma_{zx} = \frac{F}{I} \frac{2a^2}{\pi^2} \frac{\nu}{1+\nu} \sum_{n=1}^{\infty} \frac{(-1)^n}{n^2} \sin(n\pi x/a) \frac{\sinh(n\pi y/a)}{\cosh(n\pi b/a)} \tag{5}$$

$$\sigma_{zy} = \frac{F}{I} \frac{b^2 - y^2}{2} + \frac{F}{I} \frac{\nu}{1+\nu} \left[\frac{3x^2 - a^2}{6} - \frac{2a^2}{\pi^2} \sum_{n=1}^{\infty} \frac{(-1)^n}{n^2} \cos(n\pi x/a) \frac{\cosh(n\pi y/a)}{\cosh(n\pi b/a)} \right] \tag{6}$$

$$u_x = -\frac{F\nu}{EI} xyz \tag{7}$$

$$u_y = \frac{F}{EI} \left[\frac{1}{2} \nu (x^2 - y^2) z - \frac{1}{6} z^3 \right] \tag{8}$$

$$u_z = \frac{F}{EI}\left[\frac{1}{2}y(\nu x^2 + z^2) + \frac{1}{6}\nu y^3 + (1+\nu)\left(b^2 y - \frac{1}{3}y^3\right) - \frac{1}{3}a^2\nu y - \frac{4a^3\nu}{\pi^3}\sum_{n=1}^{\infty}\frac{(-1)^n}{n^3}\cos(n\pi x/a)\frac{\sinh(n\pi y/a)}{\cosh(n\pi b/a)}\right] \tag{9}$$

Test Procedure

An initial hex mesh of the beam was modeled within Cubit, and later converted to an RKPM model through the 'spheregen.py' script. The beam was meshed at four different levels of refinement: $4x4x20$, $8x8x40$, $16x16x80$, and $32x32x160$ elements.

A MATLAB script was created to read in the .genesis model data for each set of files at the four refinement levels. A specified force F was selected to produce sufficiently small strains within the beam. This F was then used to calculate the resulting displacement at each end of the beam according to the elasticity solutions, provided in the previous section. A .dat file containing this displacement data was created for each beam. A user subroutine was then implemented to read in these displacements and apply them to the ends of the beam.

From an initial zero-displacement condition at $t = 0$, the prescribed displacements at the ends of the beam were increased linearly as a function of time up to the final computed displacement values.

The 'support size' parameter included within the Sierra RKPM block required a value larger than 1.5. For consistency, this value was set to a nominal value of 1.6 for all analyses.

The time step within the RKPM model was set to match that of the FEM model, as the element sizes were effectively the same between models. This also allowed for a more comparable comparison of analysis times for each set of analyses.

Results

A visualization of the results for the prismatic beam are shown in figures 12 and 13.

The images on the left show the results for the FEM model with a mesh refinement of $8x8x40$ elements. The images on the right show the results for the RKPM model at the same refinement level. The overlapping squares depicted for the RKPM results represent individual nodes in the model. The RKPM nodes are located at the centroid of each corresponding hex element.

Visually, the displacement fields for the two models are qualitatively similar to each other. A direct comparison of displacements is not strictly feasible, as the nodes of the RKPM model do not coincide with the nodes of the FEM model. The stresses at the fixed end of the beam for the RKPM model appear to be significantly less that would they should be according to the FEM results. The

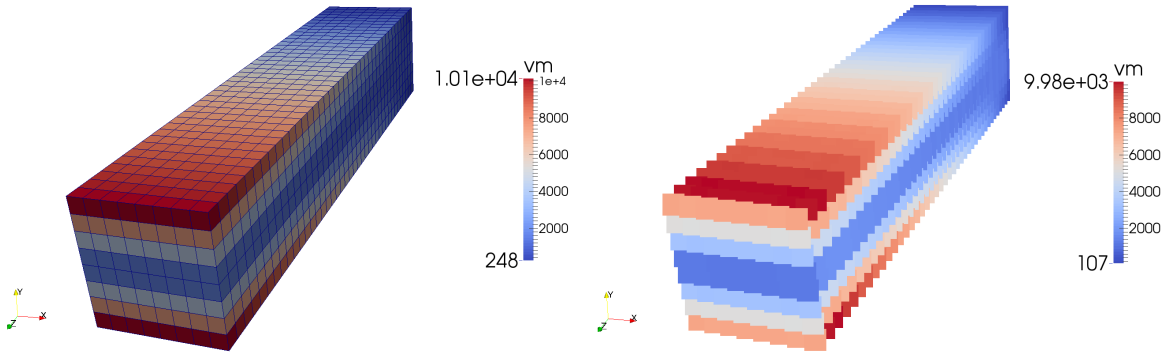

(a) **(b)**

Figure 12. Comparison of von Mises stresses in the beam for (a) FEM and (b) RKPM

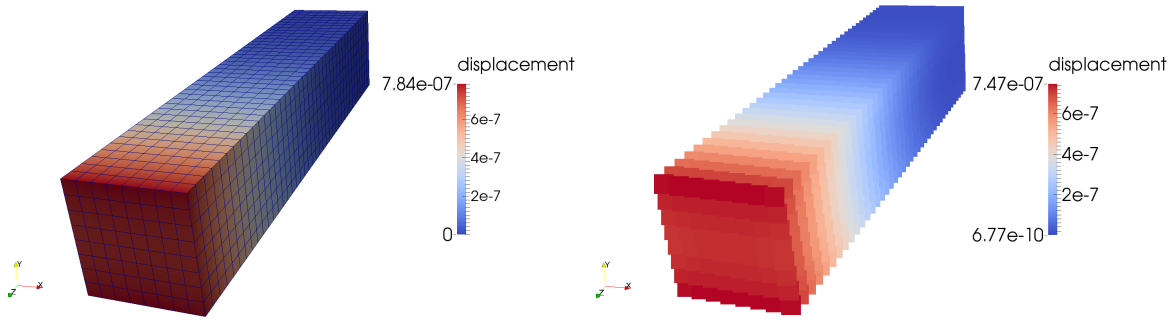

(a) **(b)**

Figure 13. Comparison of displacement magnitude in the beam for (a) FEM and (b) RKPM

magnitude of the displacements and the von Mises stresses along one of the top edges of the beam are plotted in figure 14.

The difference in node locations between the FEM and RKPM models should be taken into consideration when viewing these results. Specifically for the displacements, the nodes being referenced from the FEM model in figure 14(a) are located at a distance a and b in the x and y directions, respectively, for all refinement levels.

Since the nodes of the RKPM model are located at the centroids of the hex elements in the corresponding FEM model, the values for displacement will be different according to the displacement field at these points. As we increase mesh refinement, the locations of the nodes will become approximately coincident. Figure 14(a) makes it appear as though the displacements of the RKPM model are significantly off for lower mesh refinement levels, but this is not the case. Because the nodes are not located at the same x and y coordinates between the two models, it is not appropriate to compare FEM and RKPM displacements in this instance. Displacement errors would provide a better basis for comparison.

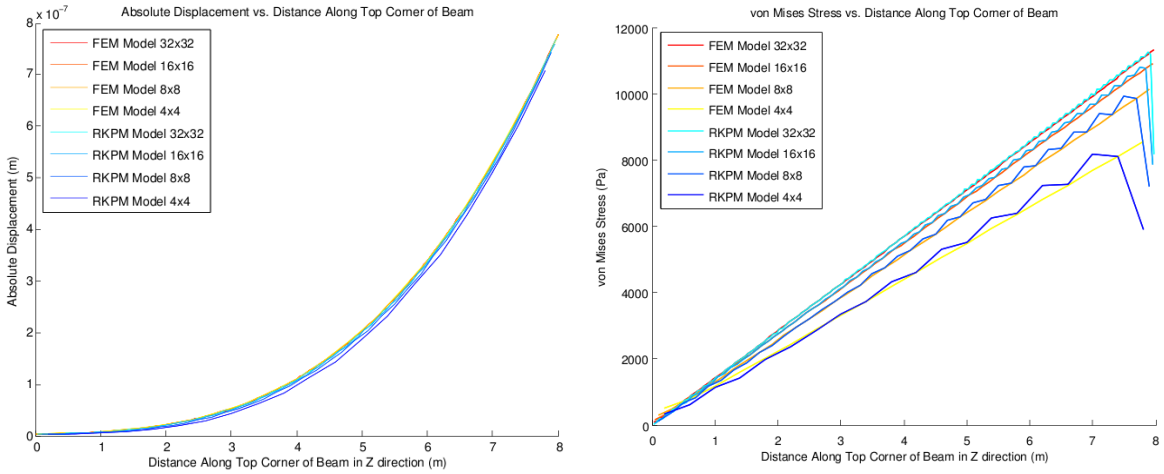

(a) **(b)**

Figure 14. Plots along top edge $(x = a, y = b)$ of beam for (a) displacement magnitude and (b) von Mises stress

Likewise for stresses, since the location of the FEM elements (and correspondingingly that of the RKPM nodes) at the top edge of the beam changes with increasing mesh refinement, so too do the stresses in these elements change. While it is not appropriate to compare between mesh refinement levels, FEM and RKPM stresses at any given level of refinement should be somewhat comparable.

From the stress plots in figure 14(b), two discrepancies are of interest: the oscillations in the RKPM stresses with wavelength 2h (where h corresponds to the size of each element) and the anomolous decrease in stresses at the fixed end of the beam where $z = L$. These phonomena were also apparent in the previous example of the axial bar, suggesting that these results may be an inidcation of a recurrent problem. It is likely that the oscillations are the result of low energy modes in the stiffness matrix. It is unclear what could be causing the decreased stress values at the end of the beam, but it may very well be linked to the application of displacement boundary conditions at these nodes in the RKPM model.

Although it is not apparent from 14(a), a closer look at the normalized absolute displacement errors in figure 15 inidcate that the oscillations described previously are also present in the displacement results. Because displacements near the 'free' end of the beam were comparatively small, a depiction of the relative percent error in the displacements would have been unrepresentative of the error magnitudes. Instead, the magnitude of the displacement error was normalized by the L^2 norm of the analytical displacements for all nodes along the top edge of the beam. This provides a relative inidcation of the percent errors for displacements, without the errors blowing up for smaller values.

The results from figure 15 are consistent with those of the axial bar problem. While the average errors and oscillations do appear to converge, it is clear from the results that the displacements

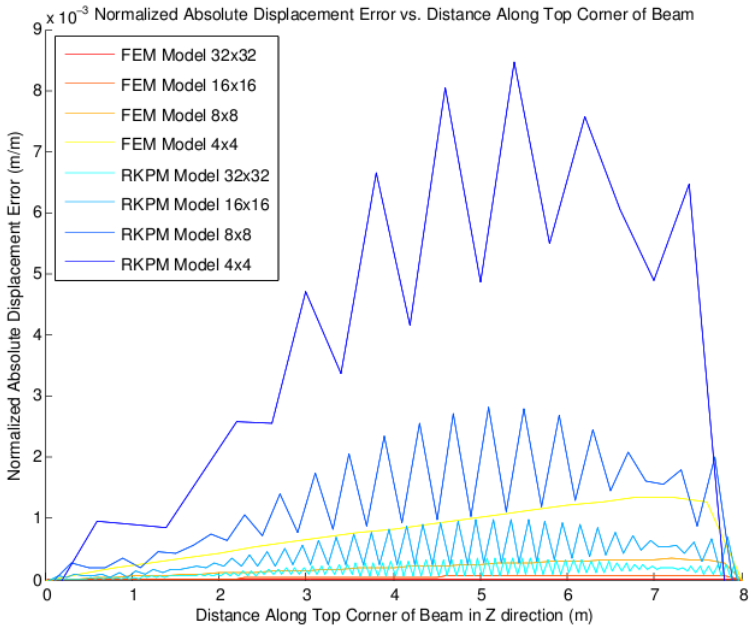

Figure 15. Absolute displacement error for nodes along the top edge of the beam, normalized by L^2 of the analytical displacements for these nodes.

obtained from RKPM are significantly less accurate than those from FEM.

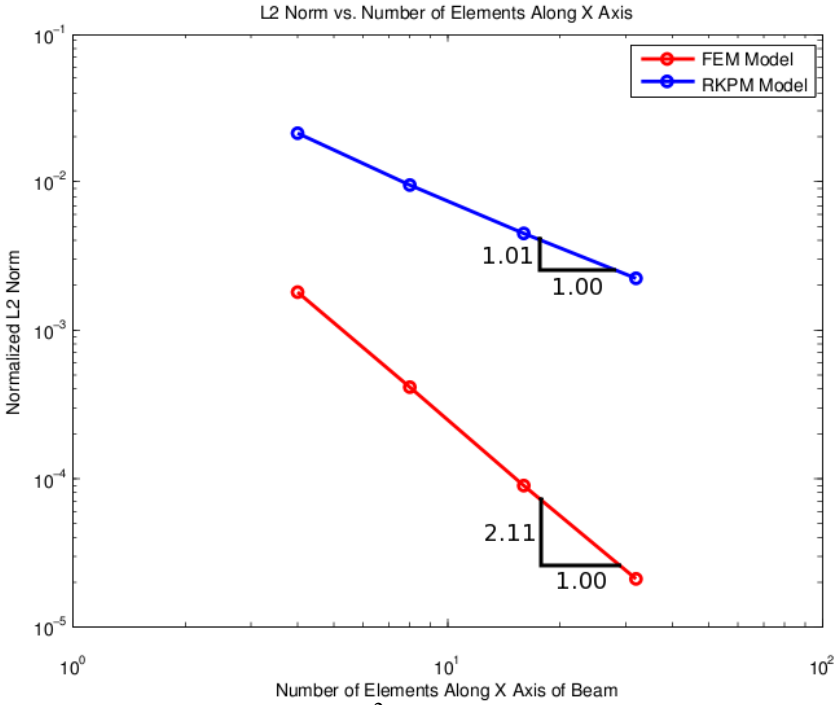

Figure 16. Normalized L^2 displacement norm vs. number of elements along the x direction of the beam.

Not only that, but it would seem that the rate of convergence in the solution is once again markedly less for RKPM. Figure 16 depicts the normalized L^2 displacement norms against increasing mesh refinement in both the FEM and RKPM models. As with the example of the axial bar, the convergence rate of the L^2 norm for RKPM is half the rate for FEM.

Energy errors were also investigated as an indicator for the error in the total stress for each element. To keep the magnitude of the energy error proportional to the stress error, the square root of the total internal energy for each element was evaluated, and then normalized by the energy norm of all elements in the domain of interest. The domain for figure 17(a) includes all elements along the top edge of the beam, resulting in a normalization of the energy error. Figure 17(b) plots the relative energy percent errors for these same elements. Together, these figures provide an indication of both the magnitude of the errors, as well as the relative percent difference from the exact solutions.

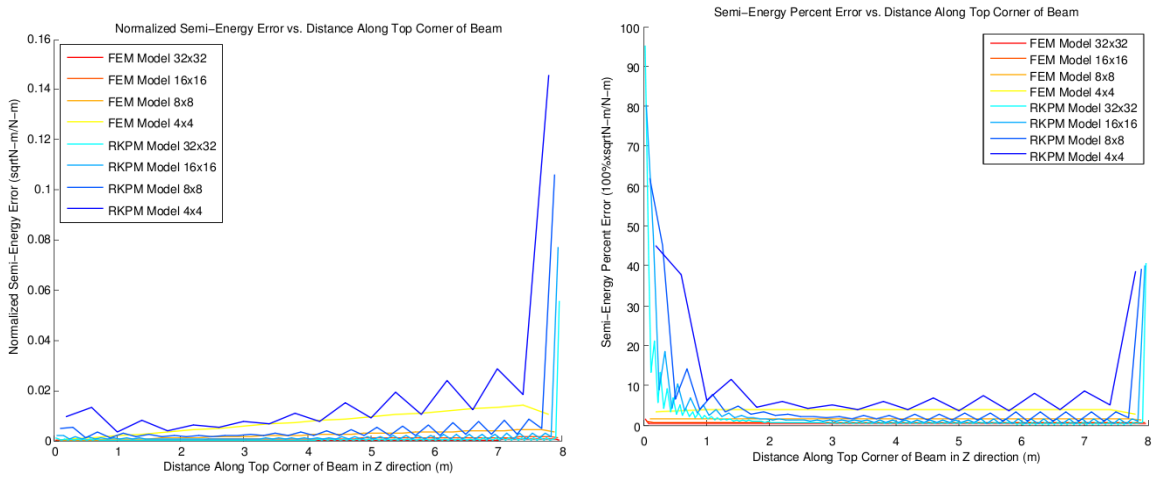

(a) **(b)**

Figure 17. Plots along top corner of beam for the (a) normalized energy error norm and (b) the pointwise norm of energy error, expressed as a percent of exact energy norm for each point

Apparent from figure 17, the energy percent errors at the ends of the beam are exceedingly large. In particular, the errors are greatest at the locations where displacement boundary conditions have been applied to the model. Based on this data and the data obtained from the previous example for the axial bar, it is clear that there is a correlation between the decreased stresses and the imposed displacement boundary conditions. Otherwise, errors in the energy elsewhere in the beam don't appear to be significantly larger than the errors obtained for the FEM soltuion.

A look at the convergence rates with increasing mesh refinement for the normalized energy norm in figure 18 show that the rate of convergence for the RKPM solution is half of what we might expect for a typical one-to-one energy norm convergence rate with FEM. Due to the way that we have defined the problem (by specifying displacement boundary conditions at both ends of the beam consistent with the exact solution for the displacement field) the observed FEM energy norm

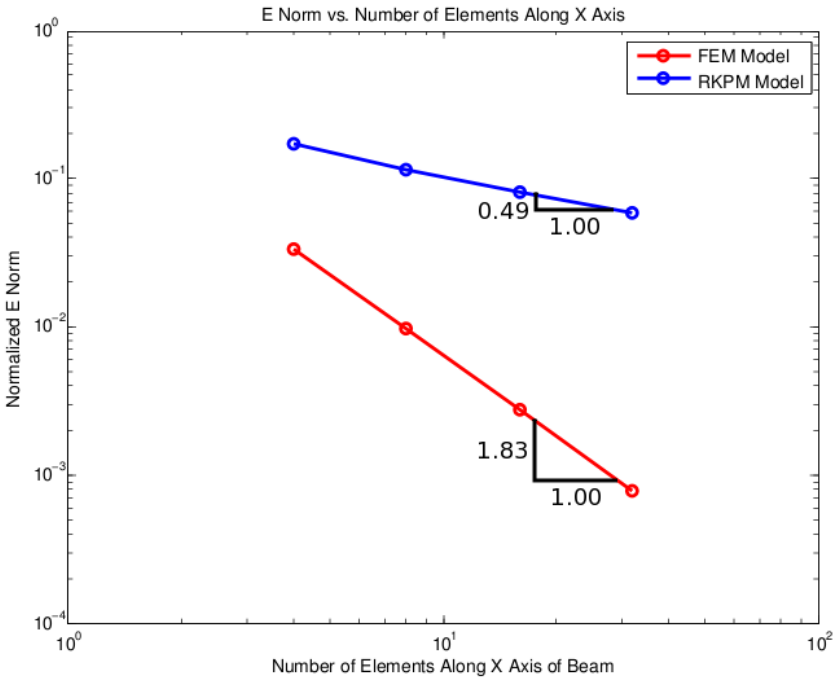

Figure 18. Normalized energy norm vs. number of elements along the x direction of the beam.

convergence rate is significantly higher than we might oridinarily expect. It is possible that this may be the result of 'superconvergence' in the FEM solution. Nonetheless, RKPM still converges at a slower rate.

Conclusions

It is encouraging to find that the values for displacement and stress obtained for the problem were at least reasonable, if perhaps not as accurate as for FEM. More importantly, convergence of the solution for RKPM was observed in both the L^2 displacement norms and the energy norms, albeit at half the typical rates for FEM. Many of the same issues observed in the previous example (such as the $2h$ wavelength oscillations in the stresses and displacements, as well as the decreased stress values at nodes contrained by displacement boundary conditions) appeared to reassert themselves in this example as well. This may inidcate that these issues are recurrent flaws within the existing implementation for RKPM.

Prismatic Shaft in Pure Torsion

Purpose

As with the previous problem, this test was intended to verify RKPM's ability to model the linear elastic material behavior of three dimensional solid bodies. The example problem in question focused on the behavior of a prismatic prismatic shaft with square cross-section subjected to pure torsion. The resulting displacement and stress fields were compared against the exact solutions from elasticity theory for infinitesimally small strains. Results are also compared against an analogous hex mesh model.

Description of Model

All model parameters for the prismatic shaft were the same as for the prismatic beam in the previous example.

The applied displacement boundary conditions were intended to induce a stress field corresponding to the application of a torque load at one end of the beam, with the opposite end fixed (weakly). Applied displacements were made sufficiently small so that the model's behavior could be closely approximated by the condition of infinitesimally small strains. The exact solutions for the resulting stress and displacement fields are provided in the following section.

As with the problem of the axial bar, the analysis was executed through Sierra/SM's explicit dynamics module (formerly Presto). The displacements at the ends of the beam were increased from zero to the absolute displacement values with a time varying linear ramp function. Viscous damping was introduced within the model to help the beam reach an approximately quasi-static condition. Sufficient time was allowed for the beam to achieve this state.

Analytical Predictions

The prismatic shaft with its corresponding coordinate system and imposed loading can be represented by the idealization in Figure 19.

Full 3-D elasticity solutions for the resulting stress and displacement fields were derived for the case of infinitesimally small strains. Analytical solutions were again provided by Dr. Joe Bishop, as referenced from his publication on polyhedral finite elements.

$$\sigma_{xx} = \sigma_{yy} = \sigma_{zz} = \sigma_{yx} = 0 \tag{10}$$

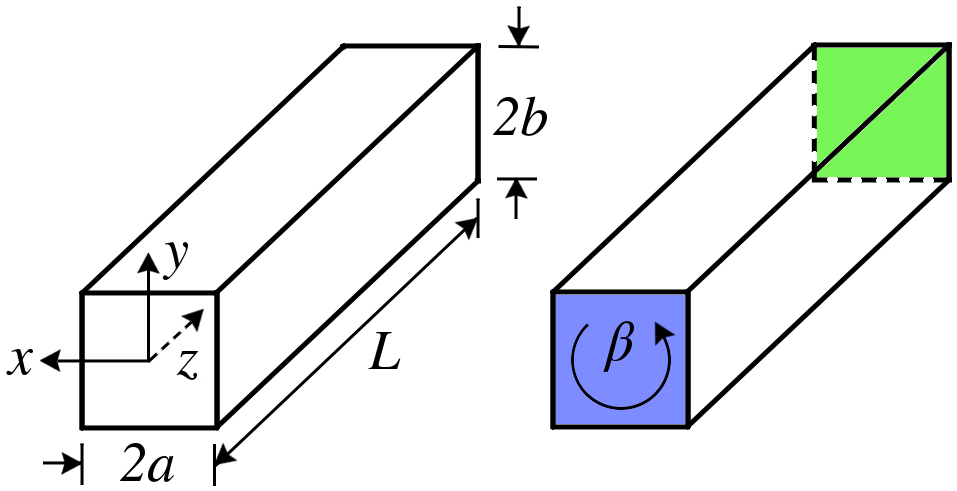

Figure 19. Prismatic Shaft Idealization: Coordinate system and relevant dimensions are depicted at left. The surface at $z = L$ (highlighted green) is fixed (weakly). The surface at $z = 0$ (highlighted blue) is subjected to a value for torque proportional to a constant, β.

$$\sigma_{zx} = \mu\beta \sum_{n=1}^{\infty} \frac{16a(-1)^n}{\pi^2(2n-1)^2} \cos\left((2n-1)\frac{\pi}{2}\frac{x}{a}\right) \frac{\sinh\left((2n-1)\frac{\pi}{2}\frac{y}{a}\right)}{\cosh\left((2n-1)\frac{\pi}{2}\frac{b}{a}\right)} \tag{11}$$

$$\sigma_{zy} = \mu\beta \left[2x + \sum_{n=1}^{\infty} \frac{16a(-1)^n}{\pi^2(2n-1)^2} \sin\left((2n-1)\frac{\pi}{2}\frac{x}{a}\right) \frac{\cosh\left((2n-1)\frac{\pi}{2}\frac{y}{a}\right)}{\cosh\left((2n-1)\frac{\pi}{2}\frac{b}{a}\right)}\right] \tag{12}$$

$$u_x = -\beta yz \tag{13}$$

$$u_y = \beta xz \tag{14}$$

$$u_z = \beta \left[xy + \sum_{n=1}^{\infty} \frac{32a^2(-1)^n}{\pi^3(2n-1)^3} \sin\left((2n-1)\frac{\pi}{2}\frac{x}{a}\right) \frac{\sinh\left((2n-1)\frac{\pi}{2}\frac{y}{a}\right)}{\cosh\left((2n-1)\frac{\pi}{2}\frac{b}{a}\right)}\right] \tag{15}$$

Test Procedure

The procedures used to model and analyze the shaft problem were identical in many respects to the methods used for the cantilever beam problem, discussed in the previous section. All relevant

model dimensions, material parameters, and analysis procedures for the shaft were the same as those used for the beam example. Mesh refinement levels were also the same.

Concerning the problem's setup, the major difference from the beam example is that of the displacement values assigned to the two ends of the shaft. Instead of a shear force F applied at one end of the beam, a chosen β proportional to the total torque applied to the shaft was used to calculate the resulting displacement field according to the elasticity solutions. The calculated displacements at the ends of the shaft were then applied to the model using the same procedure as described previously.

Results

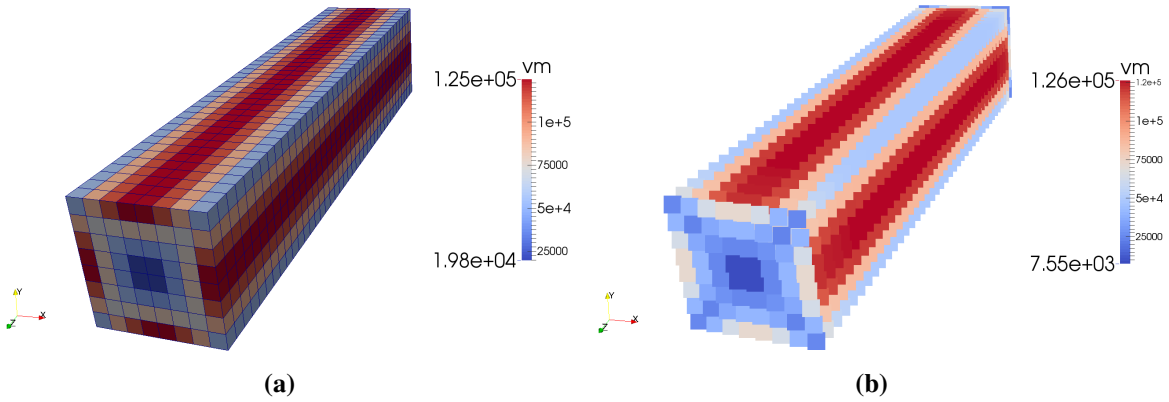

Figure 20. Comparison of von Mises stresses in the shaft for (a) FEM and (b) RKPM

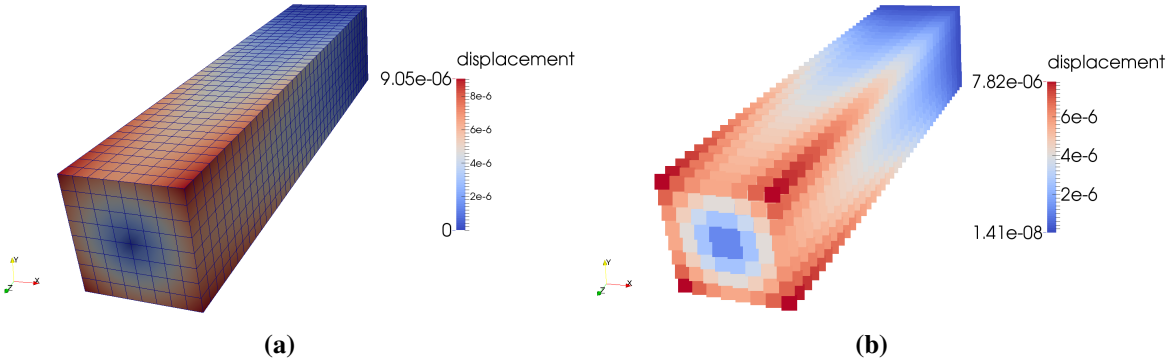

Figure 21. Comparison of displacement magnitude in the shaft for (a) FEM and (b) RKPM

A visualization of the results for the prismatic shaft are shown in figures 20 and 21.

The results are somewhat similar to what was obtained for the beam problem. Again, the stresses at the ends of the shaft for the RKPM model appear to be significantly less than what they should be according to the FEM results. The magnitude of the displacements and the von Mises stresses along the top edge of the shaft are plotted in figure 22.

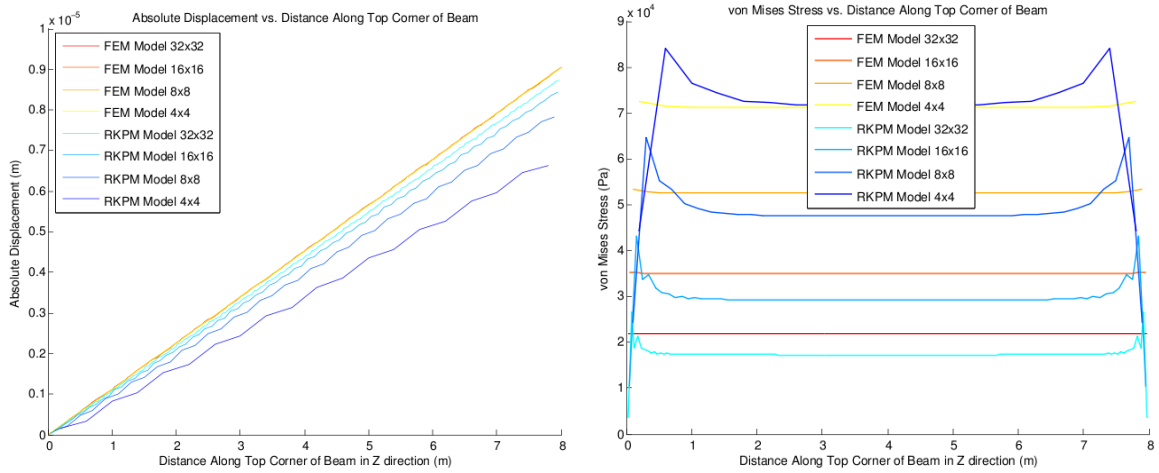

(a) **(b)**

Figure 22. Plots along top edge of beam for (a) displacement magnitude and (b) von Mises stress

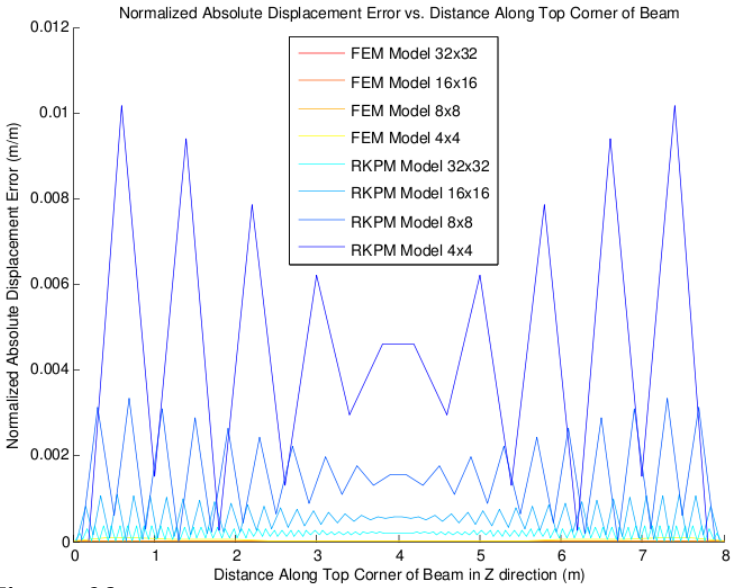

Figure 23. Absolute displacement error for nodes along the top edge of the beam, normalized by L^2 of the analytical displacements for these nodes.

Again, while the displacement fields shown in figure 22(a) for the two models are not comparable for the resasons discussed in the previous example, the stresses in figure 22(b) should be

equivalent for both RKPM and FEM.

With increasing mesh refinement, we would expect the displacements along the top edge of the beam for RKPM to approach the displacements for FEM, since the FEM nodes remain at consistent x and y locations. From the elasticity solutions, we would expect the stress at the edges of the beam to have close to zero stress. We would therefore expect to see the stress at the corners of the shaft to ultimately approach a zero value for stress.

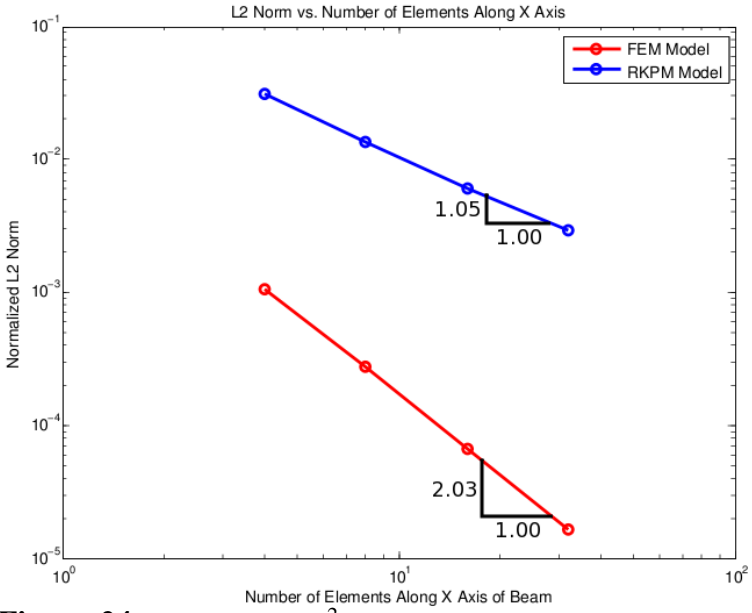

Figure 24. Normalized L^2 displacement norm vs. number of elements along the x direction of the beam.

Once more, we see from the plots in figure 22 the oscillations in the RKPM stresses and displcaments with wavelength $2h$, and the decrease in stresses at the fixed ends of the shaft where $z = 0$ and $z = L$. This time, it is more clear from the results that both ends of the beam (where displacement boundary conditions have been applied to the model) experience this decrease in stress–something that was not as apparent in the beam example.

Figure 23 depicts more clearly the oscillations in the displacement results. Similar to the beam example, the magnitude of the displacement error was normalized by the L^2 norm of the analytical displacements for all nodes along the top edge of the shaft. This provides a relative indication of the percent errors for displacements, without the errors blowing up for smaller values.

The results from figure 23 are consistent with those of the axial bar problem, and with those of the beam problem as well. Again, convergence in the solution is observed for RKPM, but the inaccuracy of the solution comapred with FEM is troubling.

Convergence rates for the shaft problem were very similar to those obtained from the previous examples. Figure 24 depicts the normalized L^2 displacement norms against increasing mesh refinement in both the FEM and RKPM models. As with the examples for the axial bar and the

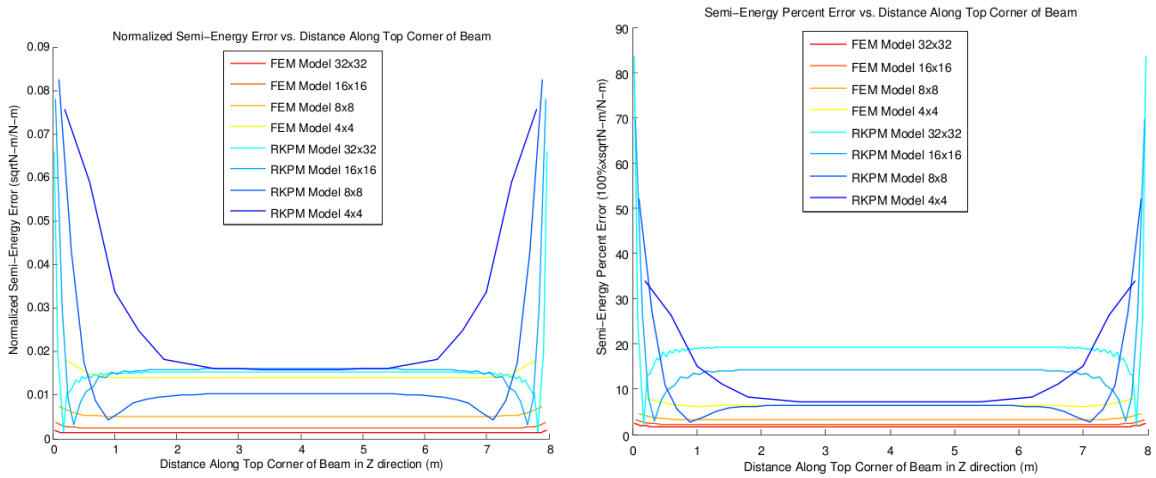

(a) **(b)**

Figure 25. Plots along top edge of beam for the square root of (a) the normalized energy error and (b) the energy relative percent error

prismatic beam, the convergence rate of the L^2 displacement norm for RKPM is roughly half the rate for FEM.

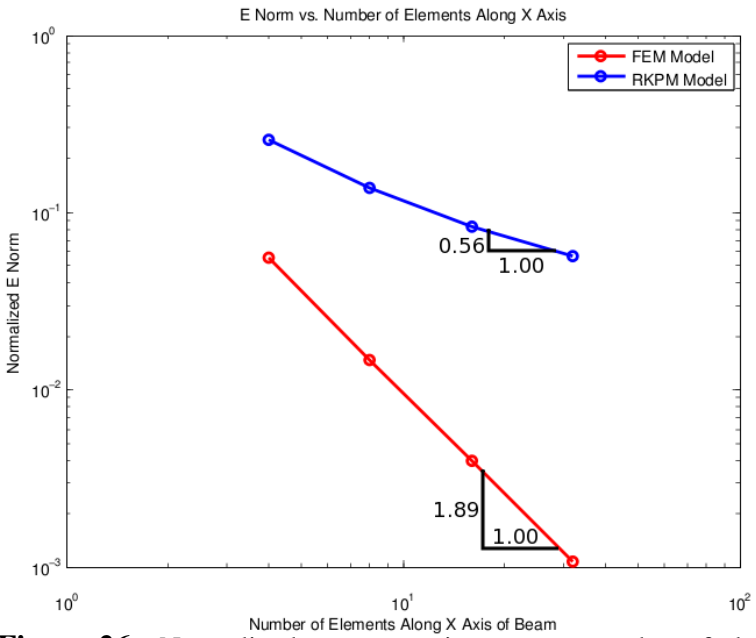

Figure 26. Normalized energy semi-norm vs. number of elements along the x direction of the beam.

Energy errors were also investigated as an indicator for the error in the total stress for each element, just as for the beam example. A similar rationale for obtaining the normalized and relative percent errors for the energy in each element yielded the plots shown in figure 25.

The energy percent errors from figure 25 are largest at the ends of the shaft, where displacement boundaries have been applied. It is likely sufficient to conclude that the errors in the stresses at the ends are indeed related to the boundary condition definitions.

Looking at the convergence rates with increasing mesh refinement for the normalized energy norm in figure 26 show that the rate of convergence for the RKPM solution is again half of what we would expect for FEM. Again, because of the way that the problem has been set up, the observed FEM energy norm convergence rate is higher than anticipated, potentially the result of 'superconvergence.'

Conclusions

The results of the torsional shaft problem appear to corroborate some of the observations made from the other tests. The results are somewhat reasonable, and convergence is obtained for increasing mesh refinement, but the issues noted in the previous examples are still present.

DISTRIBUTION:

1 MS 0899 Technical Library, 9536 (electronic copy)

This page intentionally left blank.

Sandia National Laboratories